BBA - Bioenergetics 1858 (2017) 999–1006

Contents lists available at ScienceDirect

BBA - Bioenergetics

journal homepage: www.elsevier.com/locate/bbabio

# Rhodamine-based sensor for real-time imaging of mitochondrial ATP in living fibroblasts

Diego de la Fuente-Herreruela[a,b,1], Vicente Gónzalez-Charro[a,b,1], Víctor G. Almendro-Vedia[a,b], María Morán[b,c], Miguel Ángel Martín[b,c], M. Pilar Lillo[d], Paolo Natale[a,b], Iván López-Montero[a,b,*]

[a] Dto. Química Física I, Universidad Complutense de Madrid, Avenida Complutense s/n, 28040 Madrid, Spain
[b] Instituto de Investigación Hospital "12 de Octubre" (i + 12), Avenida de Córdoba, s/n, 28041 Madrid, Spain
[c] U723, Centro de Investigación Biomédica en Red en Enfermedades Raras (CIBERER), Madrid, Spain
[d] Grupo de Fluorescencia y Biofísica Molecular, Instituto Química Física Rocasolano, CSIC, Serrano 119, 28006 Madrid, Spain

ARTICLE INFO

*Keywords:*
ATP sensor
Mitochondrial diseases
ATP mapping

ABSTRACT

Mitochondria are essential for the production and maintenance of ATP in the eukaryotic cell. To image and monitor intracellular ATP level without cell breakage, biological and chemical sensors were developed in the last years. Here, we have internalized a rhodamine-based sensor $RSL^+$ into living cells and monitored the mitochondrial ATP levels in cultured mouse embryonic fibroblasts. To evaluate the robustness of the sensor we imaged the changes of the mitochondrial ATP levels under non-physiological conditions upon incubation with FCCP, oligomycin, azide, deoxyglucose or phosphoenolpyruvate; all compounds that interfere with ATP homeostasis of the cell. The ATP sensor allowed us to determine the mitochondrial ATP levels in human skin fibroblasts where we observe a similar amount of ATP compared to mouse embryonic fibroblasts. We propose the $RSL^+$ to be a valuable tool for the assessment of mitochondrial dysfunction in human cells derived from mitochondrial OXPHOS patients and for basic studies on bioenergetics metabolism.

## 1. Introduction

In eukaryotic cells, the energetic requirements are satisfied through the synthesis of ATP inside mitochondria, where the protein complex V (ATP synthase or CV) exploits the presence of a membrane potential across the mitochondrial inner membrane established during oxidative phosphorylation (OXPHOS) [1]. An alteration of the membrane potential in the eukaryotic cell leads to mitochondrial dysfunction and appears as a common phenotype in mitochondrial diseases (MD) [2]. To evaluate and diagnose mitochondrial dysfunction, fluorescent chemical probes that surveys mitochondrial membrane potential have been developed over the past decade [3].

The majority of the probes are fluorescent lipophilic dyes based on the cationic rhodamine molecule that accumulate upon incubation within functional (negatively charged) mitochondria [4–6]. In this way, eukaryotic cells with a mitochondrial dysfunction are quickly diagnosed and identified by fluorescence microscopy [4]. Alternatively, a series of chemical sensors that detect ATP have been synthetized using zinc-based complexes such as dinuclear polyamino-phenolic-Zn(II) [7,8], Zn(II)-dipicolylamine [9,10], Zn-pyridine [11] or [Zn2L]$(ClO_4)_4$ [12] that selectively recognize phosphates but do not discriminate mono-(XMP) or di-(XDP) from triphosphates (XTP) nor distinguish purines from pyrimidines or nicotinamides. Non-homogeneous distribution of these sensors inside the cells due variable uptake efficiencies reflects a high variability of the cellular ATP concentrations.

Currently, ATP quantification is based on conventional bioluminescent assays based on the luciferin-luciferase reaction [13]. In this assay, ATP fuels the luciferase-mediated conversion of luciferin into oxyluciferin that produces chemiluminescent light that is proportional to the concentration of ATP. However, this assay requires the physical extraction of the cellular ATP and the literature reflects a large variability of the cellular ATP concentration as accurate measurements depend on the ATP extraction yield that itself depends on factors as cell culture harvesting, cell lysis, and separation steps [14].

Several strategies focus on sensors that directly image the ATP concentrations inside living cells. One strategy is to internalize a variant

*Abbreviations:* 2-DG, 2-deoxyglucose; ATP, adenosine triphosphate; FCCP, carbonyl cyanide-4-(trifluoromethoxy) phenylhydrazone; MEF, mouse embryonic fibroblasts; HSF, human skin fibroblasts; MD, mitochondrial diseases; NMR, Nuclear Magnetic Resonance; PEP, phosphoenolpyruvate; Rho123, rhodamine 123; OXPHOS, oxidative phosphorylation; ETC, electron transport chain

* Corresponding author at: Dto. Química Física I, Universidad Complutense de Madrid, Avenida Complutense s/n, 28040 Madrid, Spain.
*E-mail address:* ivanlopez@quim.ucm.es (I. López-Montero).
[1] Both authors contributed equally.

http://dx.doi.org/10.1016/j.bbabio.2017.09.004
Received 29 May 2017; Received in revised form 5 September 2017; Accepted 20 September 2017
Available online 22 September 2017

of the luciferase protein fused to a protein transduction domain (PTD-Luc), to ensure a controlled and homogenous cellular uptake of the sensor [15]. Another strategy is the development of bioluminescent sensors based on genetically encoded fluorescent reporter proteins fused to ATP binding proteins as Parceval (GFP-GlnK1) [16,17] or A-Team (CFP-$F_1$-Epsilon-YFP) [18]. These chimeric proteins are heterologously produced inside the eukaryotic cells and allow the specific real-time the measurement of the ATP concentration within an *ex vivo* tissue cell culture. Nonetheless, gene expression is particularly challenging in primary cells as it might cause their direct translation to pathological cells [19].

In this paper we present the synthesis and application of the ammonium salt of the previously reported non-charged rhodamine-based spirolactam ATP sensor (Herein: rhodamine-based spirolactam; *RSL*) [20]. The accumulation properties of cationic rhodamine-based dyes into the mitochondrial matrix will allow the real-time detection of ATP in cellular tissue cultures as mouse embryonic fibroblasts (MEF). Confocal microscopy demonstrates that $RSL^+$, the protonated form of the chemical parent, permeates the plasma membrane and senses variations of the mitochondrial ATP concentrations inside *ex vivo* tissue cultures. Ultimately, we also used $RSL^+$ to monitor ATP levels in human skin fibroblasts (HSF).

## 2. Material and methods

### 2.1. Synthesis of the $RSL^+$

Compound *RSL* was synthesized according existing literature [20]. Briefly, rhodamine B (2.00 g; 4.18 mmol) and diethylenetriamine (10 mL; 92 mmol) were dissolved in ethanol and refluxed during 24 h. After solvent evaporation under reduced pressure, the crude product was purified by silica gel column chromatography using dichloromethane:ethanol (10:1, v/v; ThermoFisher, Waltham, MA USA) as eluent solution to obtain a light pink solid product (*RSL*; Yield: 450 mg). Compound $RSL^+$ was obtained after acid-wash of *RSL* dissolved in 20 mM of $CH_2Cl_2$ with aqueous HCl (pH 3) and $RSL^+$ was recovered from the organic phase by eliminating the solvent under reduced pressure. Both compounds have been characterized by $^1$H NMR spectroscopy (CAI of NMR; Universidad Complutense Madrid) (see supplemental material).

### 2.2. UV-IR spectroscopy

UV-VIS-NIR absorption using spectra were recorded at 20 °C (Genesis 10 spectrophotometer, Fisher scientific) with a spectral bandwidth of 1.0 nm and a scan rate of 200 nm/min. All experiments were carried out using plastic cuvettes with a 1 cm optical path.

### 2.3. Fluorescence spectroscopy

Fluorescence emission spectra of compounds $RSL^+$ and *RSL* were recorded at 20 °C on a single photon counting ISS-PC1 photon counting spectrofluorimeter equipped with Glan-Taylor polarizers. Excitation wavelength was fixes at 510 nm with a slit width of 4 nm using quartz Ultra-Microcells 105.251-QS (Hellma Analytics, Germany) with a 3 × 3 cm optical path.

### 2.4. Electroformation of giant unilamellar vesicles

Giant unilamellar vesicles of 1-palmitoyl-2-oleoyl-*sn*-glycero-3-phosphocholine (POPC) lipids doped with fluorescent 1-palmitoyl-2-6-[(7-nitro-2-1,3-benzoxa diazol-4-yl) amino] hexanoyl-*sn*-glycero-3-phosphocholine (NBD-PC) were produced by electroformation [21] (Lipids were purchased from Avanti Polar Lipids, AL, USA). Briefly, 10 μL of POPC/NBD-PC (99:1 mol, 0.5 mg/mL dissolved in chloroform was spread over two conductor indium tin oxide (ITO)-coated glass slides (15–25 Ω/sq surface resistivity, Sigma Aldrich, St. Louis, MO, USA) separated 0.5 mm by a Teflon/Bytac spacer. After solvent evaporation, the fabrication chamber was sealed using Vitrex® putty (Vitrex Medical A/S, Copenhagen, DK) and the lipid films were rehydrated with a K-Buffer (30 mM KCl, 100 mM sucrose, 20 mM Mg-ATP, 5 mM $MgCl_2$) and in the presence of an AC electric field (8 Hz, 1.1 V/mm) for 2 h. Experiments were performed with 25 μL of POPC GUVs that were diluted into 50 μL of isoosmolar buffer solution (250 mM glucose, 20 mM HEPES, 1 mM KCl, pH 7,4). Prior to the addition of 15 μM valinomycin, sedimented GUVs were supplemented 35 μM of $RSL^+$. In the presence of valinomycin (Sigma Aldrich, St. Louis, MO, USA), $K^+$ ions from the lumen ($[K^+]_{in}$ = 30 mM) is transported to the external medium ($[K^+]_{out}$ = 1 mM) giving rise to an negative inside electrical transmembrane potential ($\Delta\Psi \sim log\frac{[K]_{out}}{[K]_{in}}$) [22], which triggers $RSL^+$ internalization across the lipid bilayer.

### 2.5. Cell culture

The mouse embryonic fibroblasts (3T3NIH MEF; purchased from ATCC) and human skin fibroblasts (HSF; Hospital 12 de Octubre, Madrid) were cultured in complete DMEM (high glucose Dulbecco Modified Eagle Medium), 25 mM Glucose (Gibco) supplemented with 10% fetal bovine serum (South Africa S1300; Biowest, Nuallé, France), penicillin/streptomycin (final concentration 100 U/mL of penicillin and 100 μg/mL of streptomycin respectively) and 1% of non-essential amino acids (all Gibco). The cells were grown in a humidified incubator (Forma Steri-Cycle Themofisher; 5% $CO_2$) at 37 °C and maintained, with split ratio of 1:10, at 80% of confluence in T75 flasks (Nunc).

### 2.6. Confocal fluorescence imaging of living cells

MEF were adhered at 1 × $10^4$ cells per $cm^2$ in a four-chamber Lab-Tek® slide (Thermofisher) and incubated complete DMEM for 24 h at 37 °C. Prior to confocal fluorescence imaging, adhered Mouse embryonic fibroblasts (MEFs) were supplemented either with 50 nM rhodamine 123 (Rhod123) to monitor the presence of a membrane potential or 1 μM $RSL^+$ to monitor the ATP and incubated for 60 min at 37 °C. For the co-localization, 50 nM Rhod123 and 1 μM $RSL^+$ were added simultaneously to MEFs. In addition, cells were supplemented with 25 mM HEPES medium (pH 7.4) to buffer the pH during the observation. The Lab-Tek® slide was mounted on the temperature (37 °C) controlled stage of an inverted Nikon Ti-E microscope equipped with a Nikon point scanning confocal microscope module C2, Nikon Plan Apo 100 × NA 1.45 oil immersion objective and two lasers (488 nm and 561 nm). Image capture was performed with Nikon NIS-Elements software and further processed with ImageJ [23] and Adobe Creative Suite 6 software package (Adobe Systems Incorporated). To modulate ATP homeostasis of the MEFs (N > 20), after the addition of either Rho123 or $RSL^+$ cells were supplemented individually with 1 μM carbonyl cyanide-4-(trifluoromethoxy) phenylhydrazone (FCCP), 1 μM oligomycin, 500 nM azide, 10 mM deoxyglucose (2-DG) or increasing concentrations (1 mM, 5 mM and 10 mM) of phosphoenolpyruvate. All compounds were purchased from Sigma-Aldrich St. Louis, MO, USA. Rho123 and the $RSL^+$ fluorescence were excited at 488 nm and 561 nm respectively. Collected fluorescence intensities from the confocal microscope images were corrected for laser-induced photobleaching. When appropriate, the time dependent $RSL^+$ fluorescence intensity signal decay was fitted to $I = I_0 e^{-kt + I_f}$, where $k$ is the decay rate and $I_0$ and $I_f$ account for initial and final fluorescent intensity respectively. The fluorescence decay of $RSL^+$ upon the addition of azide or deoxyglucose required a fit to a bi-exponential equation indicating two simultaneous processes responsible for the fluorescence decrease.

### 2.7. The estimation of mitochondrial ATP concentration

To quantify mitochondrial ATP concentration in living fibroblasts under physiological conditions, 4 megabyte images of the $RSL^+$ fluorescence intensity signal were captured with the Nikon NIS-Elements software and further processed with a customized MATLAB algorithm (MATLAB R2013b, MathWorks Inc.). Images were binned 2 × 2 to reduce the high level of coherent noise (laser speckle) and the fluorescence intensity signal per pixel of tens of cells (n > 20) was then converted into a concentration distribution histogram and related to a calibration standard where the fluorescence intensity of $RSL^+$ is related to the ATP concentration (Fig. S1). Within the histogram, the large contribution of the low intensity pixels (noise background) was filtered and the resulting the histogram was fitted to Gaussian distributions.

## 3. Results

### 3.1. Synthesis and spectral properties of the spirolactam ATP sensor

We synthesized the rhodamine-based spirolactam ATP sensor molecule (*RSL*) according to Li et al. [20], in order to monitor in real-time the mitochondrial ATP concentration in fibroblasts cell cultures. The ATP selectivity of the spirolactam structure is based on the assumption that hydrogen bond interaction between diethylenetriamine moiety and the polyphosphates of the ATP molecule. This interaction opens the spirolactam ring and leads to an increase of the absorption and fluorescence emission of the rhodamine B backbone molecule [24]. During the synthesis of *RSL*, we also obtained $RSL^+$, the charged ammonium salt of *RSL* (Fig. 1A; see Section 2.1 for details). The $^1$H NMR spectrum of *RSL* is in good agreement with published ATP [20] and therefore considered to be identical. Furthermore, the obtained $^1$H NMR spectrum of the charged $RSL^+$ visualizes the structural differences between *RSL* and $RSL^+$ (Fig. 1B).

First, chemical shifts corresponding to the aromatic protons (from 6 to 8 ppm) were shielded due to the presence of new protons on the tertiary amines. Second, chemical shifts ranging from 2.5 to 4 ppm that correspond to the aliphatic protons were de-shielded as consequence of the interaction with the new protons neighbouring the primary and secondary nitrogen atoms. The integration of the whole $^1$H NMR spectrum of $RSL^+$ did not result in the presence of four additional protons located in the N regions due to solvent exchange effects (Fig. 1A, red molecule). Next, we tested the spectral properties of $RSL^+$ and found them to be equivalent to those *RSL*. In the presence of 10 mM ATP, dissolved $RSL^+$ changes from a colourless solution to a light absorbing pink colour with a maximum wavelength of 560 nm (Fig. 2A and B) that increases almost linearly with an increasing ATP concentration (Fig. 2B and inset). This is not observed for 10 mM of ADP, GTP, GDP or free phosphate (Fig. 2A).The fluorescence emission of $RSL^+$ also increases with increasing ATP concentration (Fig. 2C and Fig. S1) whereas GTP, ADP and GDP only emits a small background fluorescence emission signal (39-fold, 34-fold and 63-fold respectively; inset Fig. 2D). The ATP-dependent fluorescence signal of $RSL^+$ in response to 5 to 25 mM of ATP that is almost linear form 8 mM to 20 mM of ATP (Fig. 2D).

### 3.2. Imaging of the ATP levels in mitochondria

Mouse embryonic fibroblasts (MEFs) have proven to be a powerful tool for the characterization of mitochondrial morphology and dynamics [25]. The specific labelling of the mitochondrial membrane with rhodamine 123 (Rho123) allows the direct observation of the presence of a mitochondrial membrane potential when present [26]. The internalization of the sensor molecules *RSL* and $RSL^+$ in MEFs was tested by loading them individually or together with Rho123 to cultured MEFs. The simultaneous incubation of *RSL* or $RSL^+$ with Rho123 shows that the ATP sensors localizes at the mitochondrial network. The confocal microscope images show that the charged $RSL^+$ penetrated the MEF plasma membrane and localized together with Rho123 at the mitochondrial network (Fig. 3). No defined fluorescence signal was detected for *RSL* inside cells. We conclude that the lack of charge prevents the penetration *RSL* across the plasma membrane and the further accumulation inside cell.

Additional evidence for the charge-inducing membrane permeability of compound $RSL^+$ was obtained when tested *in vitro* with giant unilamellar vesicles (GUVs) composed of POPC doped with fluorescent NBD-PC. POPC/NBD-PC-GUVs were produced in the presence of ATP, sucrose and a high-K-buffer (30 mM KCl), and then diluted into a glucose containing low-K buffer (1 mM KCl) without ATP and in the presence of 35 μM of $RSL^+$ (see Section 2.4 for details). The addition 15 μM of the selective $K^+$ transporter valinomycin to the GUVs generates a membrane potential (negative inside) [27] and $RSL^+$ enters into the lumen of the GUVs (Fig. 4A). The accumulation of $RSL^+$ inside the lumen and the detection of the ATP present is detected by an increase of the $RSL^+$ fluorescence signal (red channel). The green channel images the NBD-labelled GUV membrane, which remains unchanged throughout the experiment (Fig. 4A, bottom). Upon reversal of the polarity of the membrane potential (positive inside) (final concentration of 130 mM KCl in the external buffer), we observe a decrease of the accumulated luminal fluorescence signal as the positive charged $RSL^+$ is expelled from the lumen of the GUV.

Loading POPC/NBD-GUVs with the uncharged *RSL* under the same experimental conditions shows no internalization (Fig. 4C). To visualize the presence of the *RSL* in the external medium, a high concentration of ATP (at a final concentration of 20 mM) was added to the external medium (Fig. 4C). These experiments demonstrate that the presence of a membrane potential is necessary to accumulate $RSL^+$ inside vesicles or cells and that a fluorescence emission signal is only observed when ATP is present.

### 3.3. $RSL^+$ senses changes in ATP levels inside living mouse embryonic fibroblasts

Once we have established the membrane permeability of $RSL^+$ we needed to check its ATP sensitivity in cultured MEFs and its ability to detect alterations of the ATP concentration within mitochondria. To modulate ATP levels of the cells we added various drugs and recorded the fluorescence signals for Rho123 (green channel) and $RSL^+$ (red channel). Experiments were performed individually either in the presence of $RSL^+$ or Rho123 to avoid undesired coupling effects between both fluorophores.

In the absence of any drug, the fluorescence signal from both $RSL^+$ and Rho123 remained almost constant during recorded time interval (Fig. 5, Fig. S2). The slight decrease of fluorescence intensity of $RSL^+$ resulted from a photobleaching effect from the laser irradiation. MEFs were incubated either with carbonyl cyanide-4-(trifluoromethoxy) phenylhydrazone (FCCP), azide ($N_3^-$), oligomycin, deoxyglucose (2-DG), increasing concentrations of phosphoenolpyruvate (PEP at 1 mM, 5 mM and 10 mM) (Fig. 5) or with 2-DG in combination with increasing concentrations of PEP (at 1 mM, 5 mM and 10 mM) (Fig. S3). FCCP dissipates the membrane potential. As a consequence, Rho123 delocalizes very fast from the mitochondria and diffuses into the cytoplasm (Fig. 5 top middle and Fig. S2). The fluorescence intensity of $RSL^+$ also decreases upon FCCP treatment, although two orders of magnitude slower ($k = 10\ min^{-1}$) as compared to the fast delocalization of Rho123. Oligomycin has no effect on the membrane potential [28], but specifically blocks CV and inhibit ATP synthesis in mitochondria [29]. Upon the addition of oligomycin, the MEFs show a decrease of $RSL^+$ fluorescence signal ($k = 7.9\ min^{-1}$) and therefore the amount of mitochondrial ATP, whereas the membrane potential remains unaffected or slightly increases as CV is not able to dissipate the proton accumulation in the intermembrane space anymore (Fig. 5, top right). According to our results (see Figs. 4 and 5 top middle) the $RSL^+$ signal is

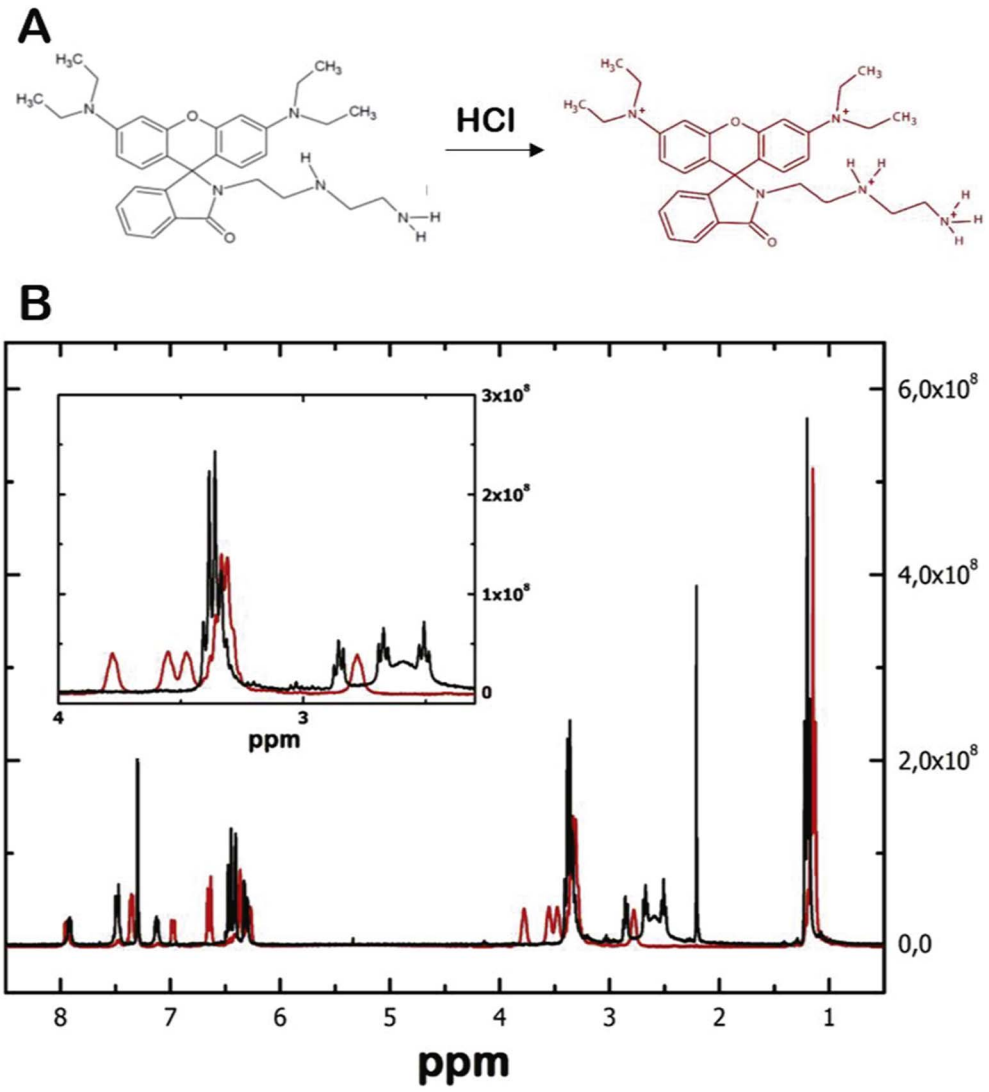


**Fig. 1.** Synthesized rhodamine based spirolactams (*RSL*): **A)** The structures of the non-charged *RSL* (black) and the charged $RSL^+$ (red) and **B)** the corresponding $^1$H-RMN spectra of the non-charged *RSL* (black line) and charged $RSL^+$ (red line) dissolved in d-chloroform.

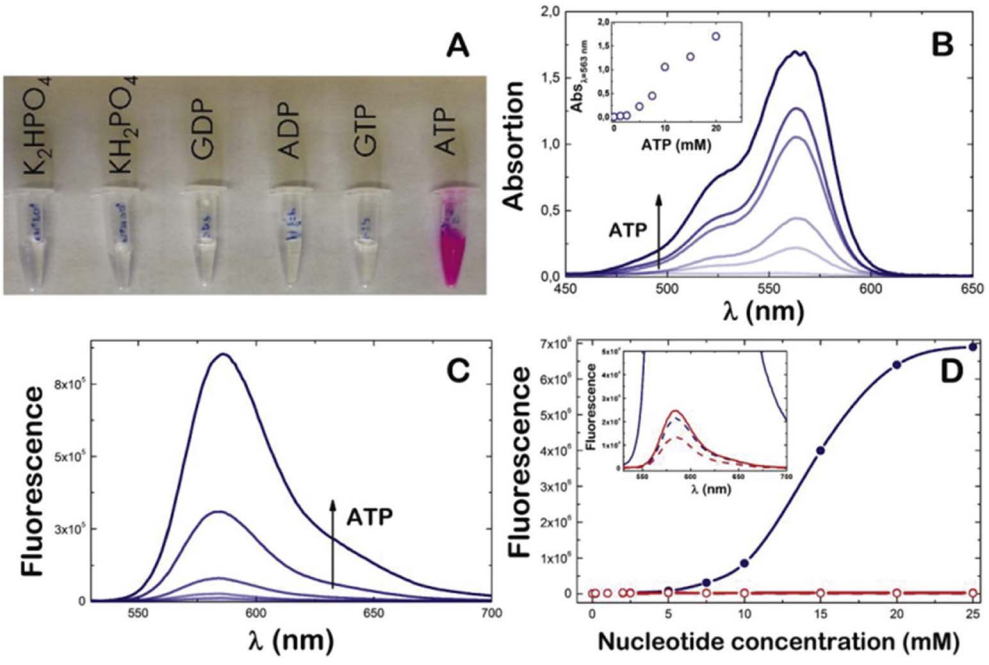


**Fig. 2. A)** The spectral properties of $RSL^+$ at a concentration of 10 μM exhibit a colour change from colourless to a light absorbing pink in the presence of 10 mM ATP, but not in the presence of 10 mM KPi, GDP, ADP or GTP. **B)** The absorption spectrum of 10 μM $RSL^+$ presents a shoulder at 520 nm and maximum at 560 nm. The absorbance depends on increasing concentration of ATP that is almost linear from 2 to 20 mM of ATP (inset). **C)** The fluorescence emission spectrum of $RSL^+$ excited at 520 nm in the presence of increasing concentration of ATP **D)** The steady-state fluorescence intensity emission of 10 μM $RSL^+$ recorded at 583 nm and excited at 520 nm in the presence of increasing nucleotide concentration (ATP blue line, ADP red line). The ATP-dependent fluorescence signal of $RSL^+$ is almost linear form 8 mM to 20 mM of ATP. Inset: The emission spectra of $RSL^+$ in the presence of ADP (red line), GTP (blue dashed line) and GDP (red dashed line) show a very weak fluorescence signal when compared to ATP (blue line).

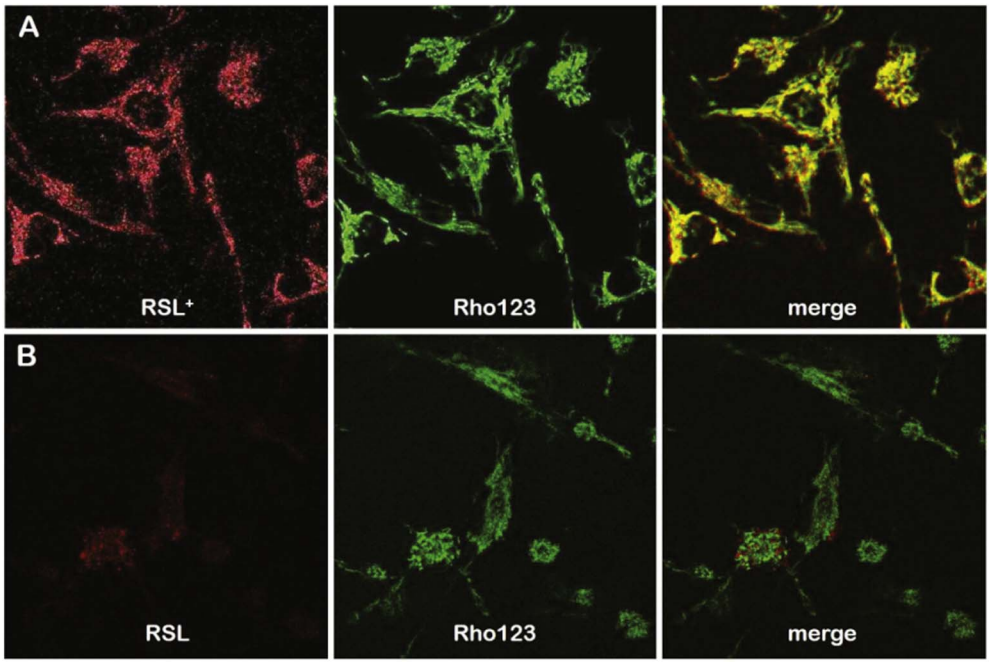


**Fig. 3.** Confocal microscope images of MEF supplemented with 1 μM *RSL* or *RSL*$^+$ (red channel) and 50 nM of Rho123 (green channel). **A)** *RSL*$^+$ penetrated the plasma membrane and localized together with Rho123 at the mitochondrial network, whereas **B)** the uncharged *RSL* penetrated the plasma membrane with very low efficiency and did not localize at the mitochondrial network but rather diffuses in the cytosol.

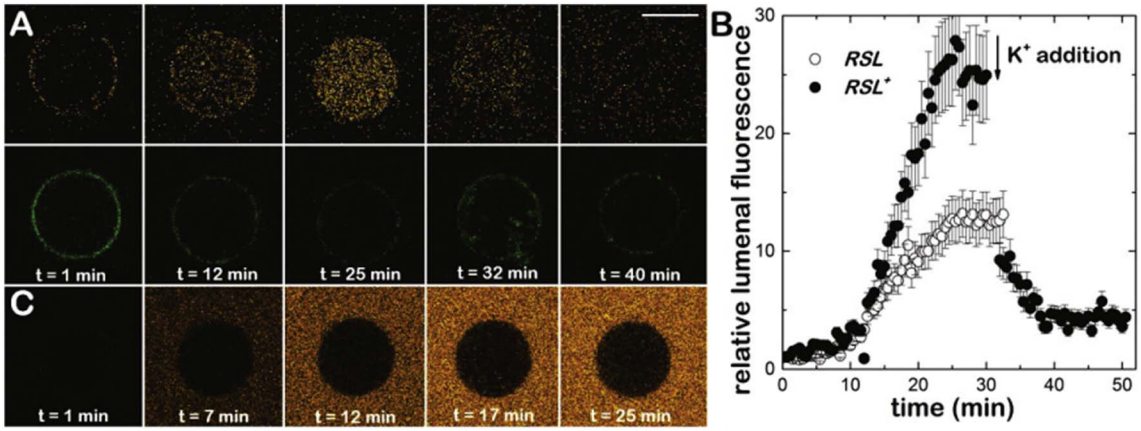


**Fig. 4.** The membrane permeability of *RSL* and *RSL*$^+$ tested in POPC-GUVs. **A)** The increase of fluorescence signal (red channel) in the lumen of the POPC-GUV containing 30 mM KCl, 20 mM ATP, 100 mM Sucrose and 5 mM $MgCl_2$; (see text for more details) indicates the accumulation of *RSL*$^+$ inside the lumen and the detection of the ATP present (see text for experimental details). No change of the fluorescence intensity (green channel) of the membrane attached NBD dye (bottom row). **B)** Time trace of the fluorescence intensity inside the POPC GUV in the presence of *RSL* or *RSL*$^+$. If we reverse the direction of the potassium transport by the addition of $K^+$ to the external buffer (at 30 min) we observe a decrease of fluorescence intensity inside the lumen. **C)** POPC-GUVs loaded with *RSL*. In this experiment, the presence of *RSL* in the external medium was visualized by the subsequent addition of ATP to a final concentration of 20 mM.

in some extent membrane potential dependent. The different fluorescent decay rate obtained with FCCP as compared to Rhodamine 123 could reflect different kinetics of the dye redistribution instead of a variation in the mitochondrial ATP levels. We performed the FCCP experiment in the presence of oligomycin, previously incubated for 10 min, to unveil if the sensor only responses to a changing membrane potential. We observed a slowing in the rate of ATP depletion without changing the rate of membrane depolarization (see Fig. S4). The actual detection of ATP levels upon membrane depolarization may lie on the different accumulation properties of the probe that change in the presence of ATP, due to the reduced charge of the sensor because of the presence of phosphates.

Next, we modulated the action of the electron transport chain by the addition of $N_3^-$, a potent inhibitor of mitochondrial respiration and produce anoxia when bound to the metal centre of complex IV (CIV) [30]. Nonetheless, $N_3^-$ also binds, although with less affinity, to CV [31] where it blocks ATP hydrolysis but not synthesis [32]. Confocal images show that the *RSL*$^+$ fluorescence intensity decreases in presence of 500 nM $N_3^-$, whereas Rho 123 fluorescence remains constant and even increases (Fig. 5, bottom left). At this concentration, $N_3^-$ inhibits CIV activity, but not completely CV. The observed decrease of *RSL*$^+$ fluorescence intensity adjusts to a second order kinetics that indicates the action of more than one process that lead to the reduction of the ATP level in the mitochondria. Next, we used 2-DG, a glucose analogue that cannot be metabolized during glycolysis and deplete the cellular pyruvate [33,34], which in turn may affect the ATP level in the mitochondria due an impairment of TCA cycle and OXPHOS function. Accordingly, we observed a reduction of the *RSL*$^+$ fluorescence signal that decreases according to a second order kinetics (Fig. 5 bottom middle). Under these conditions, the membrane potential was not affected, as glutamine, present in the complete DMEM medium, feeds into the TCA cycle *via* alpha-ketoglutarate providing succinate and the reducing equivalents NADH or $FADH_2$ to partly compensate the lack of pyruvate [28,35].

Finally, the addition of PEP at 1, 5 or 10 mM leads to an increase of *RSL*$^+$ and Rho123 fluorescence. Increasing amounts of PEP lead to

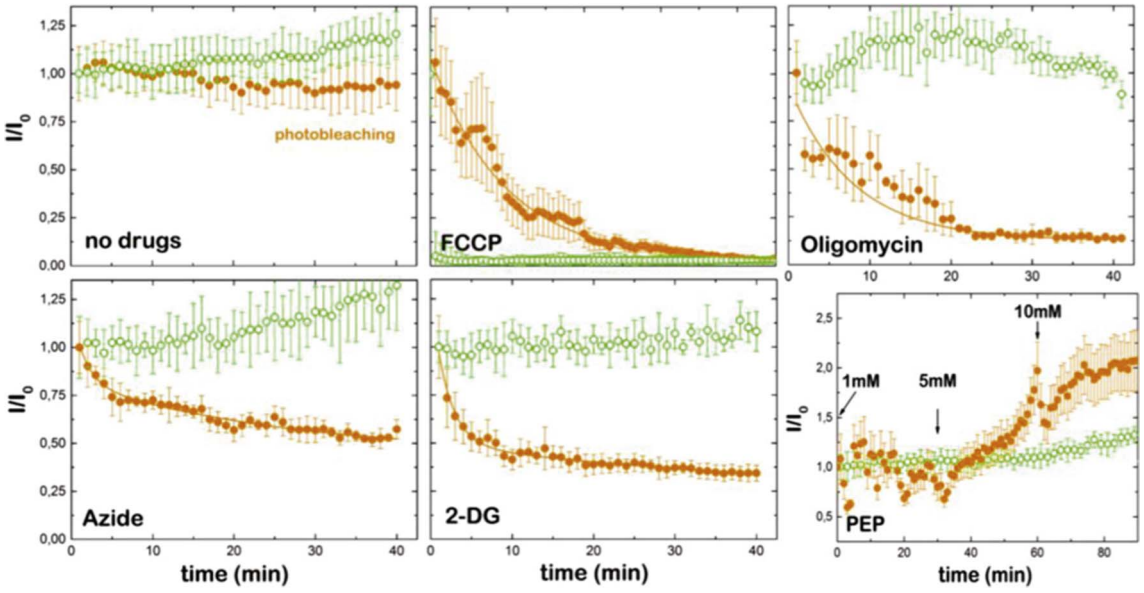


**Fig. 5.** The modulation of mitochondrial ATP levels inside MEFs. MEFs were individually supplemented either with Rho123 (membrane potential, open circles) or *RSL*$^+$ (ATP levels, closed circles) in the absence of drugs, 1 μM FCCP (carbonyl cyanide-4-trifluoromethoxy phenylhydrazone), oligomycin, $N_3^-$ (azide), 2-DG (2-deoxy-D-glucose) and PEP (phosphoenolpyruvate) (see text for details).

higher mitochondrial ATP concentration and membrane potential (Fig. 5 bottom right). If we depleted pyruvate with 2-DG prior to the addition of PEP we observed no change of the Rhod123 fluorescence intensity and a fast and intense the *RSL*$^+$ fluorescence intensity flicker (Fig. S3) indicating the rise and subsequently consumption of mitochondrial ATP. High concentration of PEP (~10 mM) retarded the ATP consumption probably introducing experimental artefacts that may lead to the production of ROS and eventually cell damage [36]. In view of all results, *RSL*$^+$ does not only sense the presence of ATP in the eukaryotic cell but is also able to distinguish differences in ATP concentrations.

### 3.4. Mitochondrial ATP levels in human fibroblasts

Biochemical studies in muscle and/or in cultured skin fibroblasts are a valuable tool in the overall evaluation of mitochondrial OXPHOS disorders [25]. In this regard, the analysis of mitochondrial ATP content could be a relevant parameter and therefore we tested *RSL*$^+$ for ATP imaging. However, our spatial intensity data resumed in the fluorescent micrographs of stained cells (Fig. 6, inset) do not give direct information about the mitochondrial ATP levels. A concentration distribution map of the fluorescence signal was generated from the corresponding calibration curves (see Fig. S1). The recorded *RSL*$^+$ fluorescence images of cells were then converted to a histogram by relating the ATP-dependent *RSL*$^+$ fluorescence intensities of the image to the ATP concentration distribution map (Fig. 6). The histogram of healthy human skin fibroblasts (HSF) incubated with *RSL*$^+$ distributes as a Gaussian curve with its maximum at an ATP concentration of 8.8 ± 1.5 mM. As a technical control, we imaged non-related *RSL*$^+$ incubated NIH3T3 MEFs and obtained a similar distribution of the fluorescence signal with a maximum at an ATP concentration of 8.5 ± 1.5 mM.

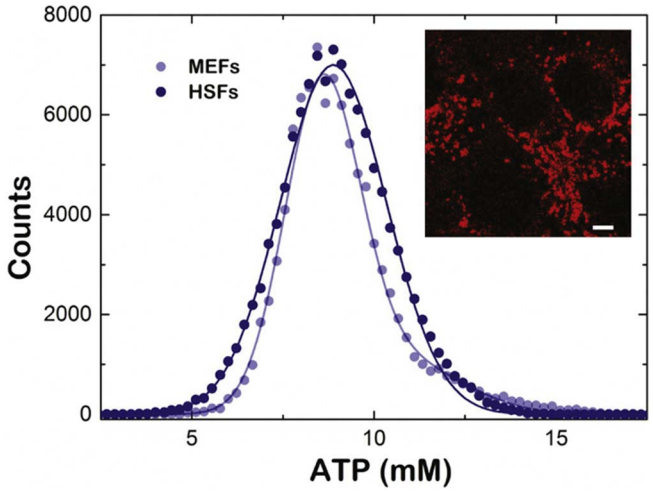


**Fig. 6.** Distribution of ATP concentration obtained from the confocal microscope images of MEFs and HSFs. The fluorescence intensity of *RSL*$^+$ intensity of fibroblasts (N = 20 each) was monitored after incubation with a *RSL*$^+$. A concentration distribution of the fluorescence signal was generated from the fluorescence intensity of individual pixels and the corresponding calibration curves (see Fig. S1). MEFs (light blue circles), HSFs (dark blue circles). **Inset**: Confocal micrographs of HSF mitochondria stained with *RSL*$^+$. Scale bar corresponds to 10 μm.

## 4. Discussion

Mitochondrial dysfunction (MD) in OXPHOS disorders is believed to be eventually caused by defective ATP production within mitochondria, which is caused by mutations in a number proteins involved in OXPHOS structure or assembly as well as in different pathways related to OXPHOS or mtDNA functioning, which are encoded both by mtDNA o chromosomal genes [37]. Due to the high phenotype variability and extreme genetic heterogeneity, diagnosis of MD is not straightforward. Although next generation genomic methods (NGS) are helping to reach more efficiently the genetic diagnosis of these disorders [38], still a great number of OXPHOS patients remain undiagnosed, and an exhaustive examination of those patients including clinical, laboratory, brain imaging findings, muscle histology, muscle and fibroblast OXPHOS biochemistry, analysis of blood and urine metabolites and finally directed genetic analysis is necessary [39,40].

We propose that the visualization of the mitochondrial ATP concentration and the simultaneous imaging of the mitochondrial dynamics in patient's skin fibroblasts could become an additional tool in the initial screen of suspected OXPHOS patients, which might lead to a straightforward identification of mitochondrial dysfunction and improve the characterization of these patients [41]. To date ATP content measurements are based on the analysis of whole cell extract, usually

cultured from patient skin fibroblast [42].

We show the real-time detection of the ATP concentration in MEFs and in HSFs using confocal microscopy in combination with rhodamine-based spirolactam ATP sensor (*RSL*; [20]). Upon the interaction with ATP, *RSL* or $RSL^+$ opens up the spirolactam-ring and display and increase in light adsorption and fluorescence emission [24]. $RSL^+$ is a membrane permeable derivative of the *RSL* compound. Membrane permeability is key for a good sensor to allow a straightforward application. The integration of the total $RSL^+$ fluorescence signal of the imaged mitochondrial network inside healthy MEFs or HSFs shows a fluorescence intensity distribution corresponding to a mitochondrial ATP concentration of 8.5 ± 1.5 mM and 8.8 ± 1.5 mM, respectively. These value almost triplicates the reported total amount of cellular ATP concentration of 3.2 ± 1.7 mM [14]. $RSL^+$ also senses, although with low affinity the nucleotides ADP, GTP and GDP (Fig. 2) whose concentration in the eukaryotic cells was determined to be 0.8 ± 0.4 mM, 0.47 ± 0.2 mM and 0.16 ± 0.05 mM, respectively [14]. These nucleotides might contribute next to ATP to the final fluorescence $RSL^+$ intensity and in this way leading to an overestimation of the cellular ATP levels. However, the high ATP specificity of $RSL^+$ and the three-fold molar excess of ATP over ADP, GTP or GDP minimizes this possibility. In addition, the fluorescence emission of $RSL^+$ is not affected by the ATP/ADP ratio but by the absolute ATP concentration (see Fig. S5). Therefore we most likely only visualize the mitochondrial ATP as $RSL^+$ specifically accumulates inside mitochondria.

It has been shown that the mitochondrial ATP concentration is twice the cytosolic ATP concentration [43]. According to our measurements, the respective cytosolic ATP concentration of our fibroblasts should be approximately 4 mM, a value that lies within the limits of reported ATP concentration. The contribution of the cytosolic ATP to the total ATP level is often biased, as in general fibroblasts are previously permealized prior to the evaluation of the cellular respiration and the cellular ATP levels [44]. As the mitochondrial matrix volume only occupies up to 35% of the cellular volume [45], cell disruption might dilute the contents of the mitochondrial matrix and mask the presence of possible local “high” ATP concentration levels. Still, inhomogeneous ATP content of individual mitochondria has been already suggested [46]. Nonetheless, in the cell, the ATP homeostasis is continuously checked and not strictly depended on the *de novo* synthesis of ATP [46].

Summed up, we show that $RSL^+$ can be used *ex vivo* for the detection of mitochondrial ATP levels of fibroblasts without the necessity of cell disruption and applied as a tool for basic research on bioenergetics. In addition, our data suggest that $RSL^+$ might be applied as a tool to diagnose MD, although a detailed study of different patient's pathologies must be evaluated.

## 5. Conclusion

In this study, we report the ability of a rhodamine-based chemosensor $RSL^+$ to image mitochondrial ATP levels with confocal fluorescence scanning microscopy. *In vitro*, $RSL^+$ shows a high selectivity for ATP over other cellular nucleotides and detects ATP concentrations from 5 to 20 mM. In cultured fibroblasts, the ATP sensor was used to monitor the variations of the mitochondrial ATP levels upon incubation with compounds that compromise the ATP homeostasis of the cell. $RSL^+$ was able to detect both decreasing and increasing ATP levels within mitochondria, independently on the presence or absence of mitochondrial membrane potential. Finally, we applied $RSL^+$ to monitor the ATP levels in HSF. Thus, the charged rhodamine-based chemosensor has demonstrated to be a valuable tool to survey cell lines and monitor the cellular energy metabolism.

## Transparency document

The Transparency document associated with this article can be found in online version.

## Acknowledgements

This work was supported by the ERC Starting Grant “mitochon” (ERC-StG-2013-338133) (I. L-M, P.N., D.F-H, V.G.C, V.G.A-V), FIS2015-70339-C2-2-R (M.P.L.) “Programa Ramón y Cajal” (RYC-2013-12609) and FIS2015-70330-C2-1-R from the Spanish Ministry of Economy MINECO (I. L-M), “Programa Miguel Servet” (CPII 16/00023) from MINECO-Instituto de Salud Carlos III (ISCIII)-FEDER to MM, and by grants to MAM (PI12/01683) and MM (PI14/01085) from MINECO, ISCIII-FEDER. We acknowledge CAI RMN (UCM) and Dr. Luis Sanchez (UCM) for technical advice on RMN spectra interpretation.

## Appendix A. Supplementary data

Supplementary data to this article can be found online at https://doi.org/10.1016/j.bbabio.2017.09.004.

## References

[1] P. Mitchell, Coupling of phosphorylation to electron and hydrogen transfer by a chemi-osmotic type of mechanism, Nature 191 (1961) 144–148.
[2] M. Zeviani, P. Fernandez Silva, V. Tiranti, Disorders of mitochondria and related metabolism, Curr. Opin. Neurol. 10 (1997) 160–167.
[3] D. Pendin, E. Greotti, K. Lefkimmiatis, T. Pozzan, Exploring cells with targeted biosensors, J. Gen. Physiol. 149 (2017) 1–36.
[4] S.W. Perry, J.P. Norman, J. Barbieri, E.B. Brown, H.A. Gelbard, Mitochondrial membrane potential probes and the proton gradient: a practical usage guide, Biotechniques 50 (2011) 98–115.
[5] J.C. Kong, C. He, X.L. Zhang, Q.T. Meng, C.Y. Duan, Rhodamine based colorimetric and fluorescent probe for recognition of nucleoside polyphosphates through multi-hydrogen bond, Dyes Pigments 101 (2014) 254–260.
[6] J.C. Smith, Potential-sensitive molecular probes in membranes of bioenergetic relevance, Biochim. Biophys. Acta 1016 (1990) 1–28.
[7] G. Ambrosi, M. Formica, V. Fusi, L. Giorgi, A. Guerri, E. Macedi, M. Micheloni, P. Paoli, R. Pontellini, P. Rossi, Phosphates sensing: two polyamino-phenolic zinc receptors able to discriminate and signal phosphates in water, Inorg. Chem. 48 (2009) 5901–5912.
[8] S. Khatua, S.H. Choi, J. Lee, K. Kim, Y. Do, D.G. Churchill, Aqueous fluorometric and colorimetric sensing of phosphate ions by a fluorescent dinuclear zinc complex, Inorg. Chem. 48 (2009) 2993–2999.
[9] A.J. Moro, P.J. Cywinski, S. Korsten, G.J. Mohr, An ATP fluorescent chemosensor based on a Zn(II)-complexed dipicolylamine receptor coupled with a naphthalimide chromophore, Chem. Commun. (Camb.) 46 (2010) 1085–1087.
[10] Y. Kurishita, T. Kohira, A. Ojida, I. Hamachi, Organelle-localizable fluorescent chemosensors for site-specific multicolor imaging of nucleoside polyphosphate dynamics in living cells, J. Am. Chem. Soc. 134 (2012) 18779–18789.
[11] A.S. Rao, D. Kim, H. Nam, H. Jo, K.H. Kim, C. Ban, K.H. Ahn, A turn-on two-photon fluorescent probe for ATP and ADP, Chem. Commun. (Camb.) 48 (2012) 3206–3208.
[12] M. Zhang, W.J. Ma, C.T. He, L. Jiang, T.B. Lu, Highly selective recognition and fluorescence imaging of adenosine polyphosphates in aqueous solution, Inorg. Chem. 52 (2013) 4873–4879.
[13] A. Lundin, A. Thore, Comparison of methods for extraction of bacterial adenine nucleotides determined by firefly assay, Appl. Microbiol. 30 (1975) 713–721.
[14] T.W. Traut, Physiological concentrations of purines and pyrimidines, Mol. Cell. Biochem. 140 (1994) 1–22.
[15] M.S. Lee, W.S. Park, Y.H. Kim, W.G. Ahn, S.H. Kwon, S. Her, Intracellular ATP assay of live cells using PTD-conjugated luciferase, Sensors-Basel 12 (2012) 15628–15637.
[16] J. Berg, Y.P. Hung, G. Yellen, A genetically encoded fluorescent reporter of ATP:ADP ratio, Nat. Methods 6 (2009) 161–166.
[17] M. Tantama, J.R. Martinez-Francois, R. Mongeon, G. Yellen, Imaging energy status in live cells with a fluorescent biosensor of the intracellular ATP-to-ADP ratio, Nat. Commun. 4 (2013).
[18] H. Imamura, K.P.H. Nhat, H. Togawa, K. Saito, R. Iino, Y. Kato-Yamada, T. Nagai, H. Noji, Visualization of ATP levels inside single living cells with fluorescence resonance energy transfer-based genetically encoded indicators, Proc. Natl. Acad. Sci. U. S. A. 106 (2009) 15651–15656.
[19] D.B. Cox, R.J. Platt, F. Zhang, Therapeutic genome editing: prospects and challenges, Nat. Med. 21 (2015) 121–131.
[20] C.Y. Li, C.X. Zou, Y.F. Li, X.F. Kong, Y. Zhou, Y.S. Wu, W.G. Zhu, A colormetric and fluorescent chemosensor for adenosine-5′-triphosphate based on rhodamine derivative, Anal. Chim. Acta 795 (2013) 69–74.
[21] V.G. Almendro Vedia, P. Natale, S. Chen, F. Monroy, V. Rosilio, I. López-Montero, iGUVs: preparing giant unilamellar vesicles with a smartphone and lipids easily extracted from chicken eggs, J. Chem. Educ. 94 (2017) 644–649.
[22] P.J. Henderson, Ion transport by energy-conserving biological membranes, Annu. Rev. Microbiol. 25 (1971) 393–428.
[23] C.A. Schneider, W.S. Rasband, K.W. Eliceiri, NIH Image to ImageJ: 25 years of image analysis, Nat. Methods 9 (2012) 671–675.

[24] H.N. Kim, M.H. Lee, H.J. Kim, J.S. Kim, J. Yoon, A new trend in rhodamine-based chemosensors: application of spirolactam ring-opening to sensing ions, Chem. Soc. Rev. 37 (2008) 1465–1472.
[25] S.A. Detmer, D.C. Chan, Functions and dysfunctions of mitochondrial dynamics, Nat. Rev. Mol. Cell Biol. 8 (2007) 870–879.
[26] L.V. Johnson, M.L. Walsh, L.B. Chen, Localization of mitochondria in living cells with rhodamine-123, Proc. Natl. Acad. Sci. Biol. 77 (1980) 990–994.
[27] P. Bhattacharyya, W. Epstein, S. Silver, Valinomycin-induced uptake of potassium in membrane vesicles from escherichia-coli - (K-uptake mutants/active transport), Proc. Natl. Acad. Sci. U. S. A. 68 (1971) 1488–1492.
[28] O. Vergun, Y.Y. Han, I.J. Reynolds, Glucose deprivation produces a prolonged increase in sensitivity to glutamate in cultured rat cortical neurons, Exp. Neurol. 183 (2003) 682–694.
[29] H.S. Penefsky, Mechanism of inhibition of mitochondrial adenosine-triphosphatase by dicyclohexylcarbodiimide and oligomycin - relationship to ATP synthesis, Proc. Natl. Acad. Sci. U. S. A. 82 (1985) 1589–1593.
[30] D. Parul, G. Palmer, M. Fabian, Ligand trapping by cytochrome c oxidase: implications for gating at the catalytic center, J. Biol. Chem. 285 (2010) 4536–4543.
[31] M.W. Bowler, M.G. Montgomery, A.G. Leslie, J.E. Walker, How azide inhibits ATP hydrolysis by the F-ATPases, Proc. Natl. Acad. Sci. U. S. A. 103 (2006) 8646–8649.
[32] D. Bald, T. Amano, E. Muneyuki, B. Pitard, J.L. Rigaud, J. Kruip, T. Hisabori, M. Yoshida, M. Shibata, ATP synthesis by F0F1-ATP synthase independent of noncatalytic nucleotide binding sites and insensitive to azide inhibition, J. Biol. Chem. 273 (1998) 865–870.
[33] E.D. Schwoebel, T.H. Ho, M.S. Moore, The mechanism of inhibition of Ran-dependent nuclear transport by cellular ATP depletion, J. Cell Biol. 157 (2002) 963–974.
[34] A.N. Wick, D.R. Drury, H.I. Nakada, J.B. Wolfe, Localization of the primary metabolic block produced by 2-deoxyglucose, J. Biol. Chem. 224 (1957) 963–969.
[35] O.E. Owen, S.C. Kalhan, R.W. Hanson, The key role of anaplerosis and cataplerosis for citric acid cycle function, J. Biol. Chem. 277 (2002) 30409–30412.
[36] A.A. Starkov, G. Fiskum, C. Chinopoulos, B.J. Lorenzo, S.E. Browne, M.S. Patel, M.F. Beal, Mitochondrial alpha-ketoglutarate dehydrogenase complex generates reactive oxygen species, J. Neurosci. 24 (2004) 7779–7788.
[37] W.C. Copeland, Inherited mitochondrial diseases of DNA replication, Annu. Rev. Med. 59 (2008) 131–146.
[38] C.J. Carroll, V. Brilhante, A. Suomalainen, Next-generation sequencing for mitochondrial disorders, Br. J. Pharmacol. 171 (2014) 1837–1853.
[39] M.A. Kirkman, P. Yu-Wai-Man, P.F. Chinnery, The clinical spectrum of mitochondrial genetic disorders, Clin. Med. 8 (2008) 601–606.
[40] N.I. Wolf, J.A.M. Smeitink, Mitochondrial disorders - a proposal for consensus diagnostic criteria in infants and children, Neurology 59 (2002) 1402–1405.
[41] R.J.T. Rodenburg, Biochemical diagnosis of mitochondrial disorders, J. Inherit. Metab. Dis. 34 (2011) 283–292.
[42] J.M. Cameron, V. Levandovskiy, N. MacKay, B.H. Robinson, Respiratory chain analysis of skin fibroblasts in mitochondrial disease, Mitochondrion 4 (2004) 387–394.
[43] C.D. Gajewski, L.C. Yang, E.A. Schon, G. Manfredi, New insights into the bioenergetics of mitochondrial disorders using intracellular ATP reporters, Mol. Biol. Cell 14 (2003) 3628–3635.
[44] O. Guillery, F. Malka, P. Frachon, D. Milea, M. Rojo, A. Lombes, Modulation of mitochondrial morphology by bioenergetics defects in primary human fibroblasts, Neuromuscul. Disord. 18 (2008) 319–330.
[45] M.M. Anastacio, E.M. Kanter, C.M. Makepeace, A.D. Keith, H. Zhang, R.B. Schuessler, C.G. Nichols, J.S. Lawton, Relationship between mitochondrial matrix volume and cellular volume in response to stress and the role of ATP-sensitive potassium channel, Circulation 128 (2013) S130–S135.
[46] D.C. Liemburg-Apers, H. Imamura, M. Forkink, M. Nooteboom, H.G. Swarts, R. Brock, J.A.M. Smeitink, P.H.G.M. Willems, W.J.H. Koopman, Quantitative glucose and ATP sensing in mammalian cells, Pharm. Res. Dordr. 28 (2011) 2745–2757.